Charge, orbital, and magnetic order in $Nd_{0.5}Ca_{0.5}MnO_3$

F. Millange,[1,*] S. de Brion,[2,†] and G. Chouteau[2]
[1]*CRISMAT-ISMRA, CNRS and Université de Caen 6, Boulevard du Maréchal Juin, 14050 Caen, France*
[2]*Grenoble High Magnetic Field Laboratory, Boîte Postale 166, 38042 Grenoble Cedex 9, France*
(Received 20 December 1999; revised manuscript received 5 May 2000)

In the manganite $Nd_{0.5}Ca_{0.5}MnO_3$, charge ordering occurs at a much higher temperature than the antiferromagnetic order ($T_{CO}=250$ K, $T_N=160$ K). The magnetic behavior of the phase $T_N<T<T_{CO}$ is puzzling: its magnetization and susceptibility are typical of an antiferromagnet while no magnetic order is detected by neutron diffraction. We have undertaken an extensive study of the crystallographic, electric, and magnetic properties of $Nd_{0.5}Ca_{0.5}MnO_3$ and established its phase diagram as a function of temperature and magnetic field. The charge disordered paramagnetic phase above T_{CO} presents ferromagnetic correlations. An antiferromagnetic charge exchange phase prevails below T_N, with complete charge and orbital ordering. In the intermediate temperature range, charge ordering occurs while orbital ordering sets in progressively, with no magnetic order. Strong magnetic fields destroy the charge ordered phases in a first-order transition towards a ferromagnetic state.

I. INTRODUCTION

The manganites $L_{1-x}M_xMnO_3$, where L is a trivalent rare earth and M a divalent alkaline earth element, present astonishing properties due to the interplay of magnetism, electric transport, and crystallographic distortion. Much interest has been focused on the hole doped ferromagnetic phase ($x\simeq0.3$) that exhibits colossal magnetoresistance.[1] At fractional doping level, another mechanism is superimposed: charge ordering between Mn^{3+} and Mn^{4+} ions takes place.[2–5] The crystallographic and magnetic environment is then strongly modified. For instance, $Nd_{0.5}Sr_{0.5}MnO_3$ (Refs. 3 and 5) is ferromagnetic and metallic below 245 K. At 160 K, the charge order transition occurs and the system becomes antiferromagnetic and insulating. Applying a strong magnetic field restores the ferromagnetic order together with the metallic conductivity.

However, these properties depend crucially on the local lattice distortion and the mismatch between the rare earth and the alkaline element.[6,7] In these perovskite structures, it is convenient to define the tolerance factor $t=(r_{L,M}+r_O)/\sqrt{2}(r_{Mn}+r_O)$ where $r_{L,M}$, r_{Mn}, and r_O are the average ionic radii of the trivalent rare earth and divalent alkaline earth site, manganese site, and oxygen site, respectively. It describes the distortion of the perovskite structure. This distortion modifies the strength of the different magnetic interactions present in these systems. The double exchange mechanism[8] couples the itinerant $3de_g$ electrons of Mn^{3+} with the localized $3dt_{2g}$ spins of the Mn^{4+} ions. It favors ferromagnetism together with metallic conductivity. It depends on the number of e_g electrons as well as the bond angle Mn-O-Mn governed by the lattice distortion. On the other hand, the superexchange interaction between manganese ions favors antiferromagnetic order with localized spins with then insulating electric properties. Decreasing the ionic radius of the L and M site modifies the bond angle Mn-O-Mn. The ferromagnetic ordering interaction is then reduced.[6] The bandwidth of the e_g electron becomes narrower. Eventually, the system becomes insulating and loses its ferromagnetic order.

Additionally, for $x=0.5$, charge ordering will tend to localize the spins and destabilize the ferromagnetic order. This is what has been observed in $Nd_{0.5}Sr_{0.5}MnO_3$ (Ref. 3) and in $Pr_{0.5}Sr_{0.5}MnO_3$ (Ref. 2) where the tolerance factor is close to 0.95. The ferromagnetic metallic order established below $T_C\approx250$ K, is destroyed when charge ordering sets in at $T_{CO}\approx150$ K, and the system becomes antiferromagnetic and insulating ($T_N=T_{CO}$).

For smaller tolerance factor, the magnetic phase diagram is not so clear. In $Pr_{0.5}Ca_{0.5}MnO_3$,[9,10], with $t=0.933$, or in $Sm_{0.5}Ca_{0.5}MnO_3$ ($t=0.924$),[4] the charge order state occurs at higher temperature ($T_{CO}\approx250$ K) so that no ferromagnetic order is established in zero magnetic field. Antiferromagnetism is observed only at lower temperature ($T_N\approx150$ K $<T_{CO}$).

Surprisingly, the magnetic susceptibility presents a huge peak at T_{CO}, as observed for a long-range antiferromagnetic order, and none at T_N. Such a behavior is very sensitive to stoichiometry. In $Pr_{0.6}Ca_{0.4}MnO_3$,[9,11] as well as in $Nd_{0.6}Ca_{0.4}MnO_3$,[12] the anomaly at T_{CO} persists while the signature of T_N is quite visible. What is the exact nature of the phase when $T_N<T<T_{CO}$? What is the mechanism responsible for the susceptibility anomaly at T_{CO}? To answer these questions, we have focused on the compound $Nd_{0.5}Ca_{0.5}MnO_3$ for which $t=0.930$. We have undertaken an extensive study of its crystallographic, electric, and magnetic properties using neutron diffraction, electric transport, magnetic susceptibility, and high-field magnetization measurements.

II. EXPERIMENTS

The powdered sample was prepared by solid-state reaction from the component oxides in appropriate ratios. The reagents were intimately mixed in an agate mortar and heated in air at 900 °C for 12 h to allow decarbonation to take place. This powder was fired at 1200 °C for 12 h. Final

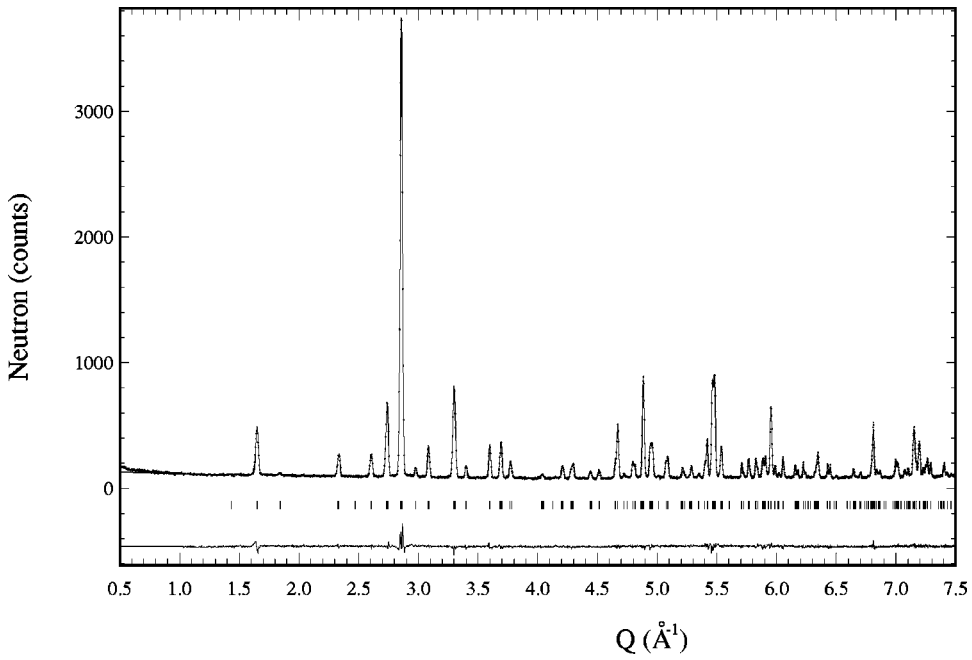

FIG. 1. Rietveld refinement plot of the neutron-diffraction data at room temperature. The ticks are given for the nuclear structure peaks.

firing was performed at 1500 °C for 5 days with intermediate grinding to ensure homogeneity. Phase purity was checked by x-ray diffraction using a Phillips diffractometer with Cu-K_α radiation.

The phase $Nd_{0.5}Ca_{0.5}MnO_3$ was subsequently registered on the high-resolution diffractometer D2b at the Institut Laue Langevin using a wavelength of $\lambda = 1.5938$ Å at room temperature and 1.5 K. The sample was contained in a vanadium can. The high-flux powder diffractometer CRG-CNRS D1b was used to investigate the thermal dependence of the magnetic structure in the temperature range 1.5−293 K. Thanks to the position sensitive detector covering 80°(2θ) and the high neutron flux available at the 2.52, Å wavelength, a neutron diffraction pattern has been measured every 6 K. The nuclear and magnetic refinement were performed using the profile fitting program FULLPROF[13] ($b_{Mn} = -0.373 \times 10^{-12}$ cm, $b_O = 0.580 \times 10^{-12}$ cm, $b_{Nd} = 0.769 \times 10^{-12}$ cm, $b_{Ca} = 0.470 \times 10^{-12}$ cm).

Magnetic susceptibility measurements were made with a superconducting quantum interference device magnetometer (MPMS quantum design) in the temperature range 4–350 K. These dc susceptibility measurements were carried out at low field (10 mT) with increasing temperature after the samples were either zero-field cooled or field cooled. High-temperature susceptibility measurements were also taken up to 800 K using a Faraday balance. High-field magnetization measurements were performed, up to 22 T, with a conventional extraction setup, in the temperature range 4–300 K.

The electric resistivity was measured between 5 and 600 K, using a standard four- points method, on a bar with typical dimensions $0.2 \times 0.2 \times 1$ cm^3. Magnetoresistance measurements were performed with magnetic fields up to 7 T, the temperature ranging from 5 to 400 K.

III. RESULTS

A. Neutron diffraction

The powder neutron diffraction pattern of $Nd_{0.5}Ca_{0.5}MnO_3$, collected at room temperature in the paramagnetic domain, exhibits the orthorhombic $GdFeO_3$ structure ($a \approx a_p\sqrt{2}$, $b \approx 2a_p$, $c \approx a_p\sqrt{2}$). Refinements of the room-temperature neutron diffraction patterns carried out in the space group *Pnma* attest the validity of the structure resolution. The data were first analyzed with a ''whole pattern fitting'' algorithm in order to determine accurately the profile shape function, background, and cell parameters. This preliminary study provided a good estimate of the R_{wp} and χ^2 that could be reached during the structure refinement. This whole pattern fitting led to an agreement factor $R_{wp} = 4.48\%$ and $\chi^2 = 1.42$. The refinement was undertaken with the room-temperature neutron-diffraction pattern, a temperature for which the magnetic measurements showed a paramagnetic behavior (see the magnetic properties section). 235 Bragg peaks were used to refine seven positional parameters and four isotropic temperature factors. The refinement converged to give an agreement factor $R_{wp} = 4.84\%$ and $\chi^2 = 1.71$. Observed, calculated, and difference diffraction profiles are shown in Fig. 1. A Jahn-Teller (J-T) distortion of the Q_2 type (antiferrodistorsive), which displaces the basal plane oxygen atoms from their ideal positions, has been proposed to be responsible for the insulating state. This distortion does not change the lattice symmetry (*Pnma*) but modifies the cell deformation in such a way that $b/\sqrt{2} \leqslant c \leqslant a$ (the O'-type structure). Thus, the resulting Mn-O bond lengths of 1.943 Å and 1.948 Å (basal plane) and 1.936 Å (apical distance) at room temperature are at the origin of a small gap between the J-T split Mne_g bands ($d_{x^2-y^2}$ and d_{z^2}).

On cooling the specimen $Nd_{0.5}Ca_{0.5}MnO_3$ below 250 K, very weak extra reflections appear on the electron microdiffraction patterns.[14] The patterns can only be indexed by doubling the *a* lattice parameter. However, the extra reflections are too weak to determine the point group from electron microdiffraction patterns and from convergent beam electron-diffraction patterns. Therefore, subsequent refinements based on neutron diffraction data were carried out in

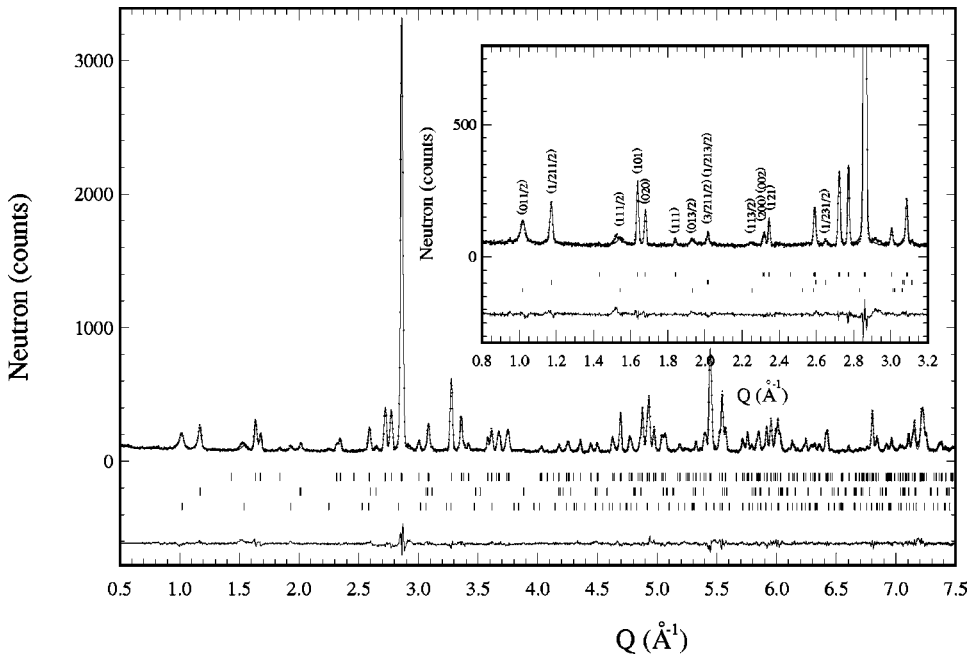

FIG. 2. Rietveld refinement plot of the neutron-diffraction data at 1.5 K. The ticks are given for the nuclear structure peaks (upper), magnetic structure peaks (Mn^{4+} sublattice, middle), and magnetic structure peaks (Mn^{3+} sublattice, lower). Points are the experimental data, line is the Rietveld fit, and the lower line is the difference curve.

the higher symmetry *Pnma* space group, characteristic of the structure above the transition (see Fig. 2). It should be clear that this procedure will yield only a structure averaged over the symmetry operators of the *Pnma* space group. Refinements of a *Pnma* model lead to large displacement parameters of the oxygen atoms indicative of disorder and/or subtle distortions not taken into account by an orthorhombic model. The corresponding $Nd_{0.5}Ca_{0.5}MnO_3$ structural parameters, selected bond distances, and angles at room temperature and 1.5 K are reported in Table I. The most significant difference between the room-temperature and the low-temperature structures is in the Mn-O bond lengths. At room temperature, the octahedral coordination of manganese with oxygen is almost undistorted, with six approximately equal Mn-O distances. At low temperature, the two Mn-O_1 distances (along the *b* axis) become shorter than the four Mn-O_2 distances in the *a*-*c* plane, implying a J-T distortion of the ''apically compressed'' type as previously reported by Radaelli *et al.*[15] in $La_{0.5}Ca_{0.5}MnO_3$. The mean distortion in the MnO_6 octahedra Δ_d is increased by a factor of 20 as the temperature decreases from room temperature to low temperature. These results clearly demonstrate that there is a close link between the lattice parameters and the presence of the J-T distorted $Mn^{3+}O_6$ octahedra with the d_{z^2} orbital oriented in the *a*-*c* plane.

The high-flux powder diffractometer D1b was first used to investigate the thermal dependence of the orthorhombic cell parameters in the temperature range of 1.5–293 K (Fig. 3). One observes that *a* and *c* parameters increase as the temperature is lowered from $T_{CO}=250$ K to $T=160$ K accompanied by a significant decrease in the *b* parameter. Our results demonstrate that the charge ordered state is progressively established from $T_{CO}=250$ K to $T=160$ K.

The magnetic reflections in the low-temperature neutron powder-diffraction pattern have been indexed on the basis of $(a\approx a_p\sqrt{2},\ b\approx 2a_p,\ c\approx a_p\sqrt{2})$ unit cell, previously reported by Wollan and Koehler.[16] The magnetic structure of $Nd_{0.5}Ca_{0.5}MnO_3$, known as charge-exchange (CE) type (Fig. 4), is quite complex: it entails a quadrupling of the volume of the original orthorhombic unit cell and consists of two magnetic sublattices with independent propagation vectors. This observation, associated with the fact that $Nd_{0.5}Ca_{0.5}MnO_3$ is an insulator (see electrical properties below), has confirmed the hypothesis, first formulated by Goodenough[17] and developed by others,[18] that the two sublattices result from charge ordering between Mn^{3+} and Mn^{4+}. In Goodenough's model, charge ordering is accompanied by orbital ordering forming ferromagnetic zigzag chains in the *a*-*c* plane (d_{z^2} Mn^{3+} orbitals associated with the long Mn^{3+}-O bonds in the J-T distorted $Mn^{3+}O_6$ octahedra). These ferromagnetic chains are connected antiferromagnetically to each other in the *a*-*c* plane and along the *b* axis. The magnetic structures of the two sublattices have different propagation vectors: $\vec{k}_1=(0,0,1/2)$ for Mn^{3+} and $\vec{k}_2=(1/2,0,1/2)$ for Mn^{4+}. Rietveld refinements of the low-temperature neutron powder-diffraction pattern clearly indicate that the magnetic moments are oriented along the *a* axis (Fig. 5). The refined values of the magnetic moments at 2 K are reported in Table II while their temperature variations are plotted in Fig. 4. Above $T_N=160$ K, this magnetic moment vanishes. It is worth noticing that the long-range antiferromagnetic order is established only well below T_{CO}. It is important to note here that T_N exactly coincides with the temperature below which the lattice parameters become constant (Fig. 3).

B. Electrical properties

The electric resistivity $\rho(T)$ is plotted in Fig. 6. The compound remains insulating whatever the temperature. Below 50 K, the resistivity is too high to be measured. Such an

TABLE I. $Nd_{0.5}Ca_{0.5}MnO_3$ structural parameters at room temperature (RT) and 1.5 K, as determined from Rietveld refinements based on neutron powder-diffraction data.

$Nd_{0.5}Ca_{0.5}MnO_3$ at RT				$Nd_{0.5}Ca_{0.5}MnO_3$ at 1.5 K			
Cell parameters				*Cell paramaters*			
$a=5.4037(1)$ Å				$a=5.4354(1)$ Å			
$b=7.5949(1)$ Å				$b=7.4832(1)$ Å			
$c=5.3814(1)$ Å				$c=5.4157(1)$ Å			
Atomic coordinates				*Atomic coordinates*			
	x	*y*	*z*		*x*	*y*	*z*
Nd/Ca	0.0322(2)	0.25	−0.0054(4)	Nd/Ca	0.0349(2)	0.25	−0.0057(4)
Mn	0	0	0.5	Mn	0	0	0.5
O1	0.4876(4)	0.25	0.0690(3)	O1	0.4862(3)	0.25	0.0722(4)
O2	0.2860(3)	0.0361(2)	−0.2856(2)	O2	0.2886(2)	0.0375(2)	−0.2859(2)
Mn-O distances				*Mn-O distances*			
Mn-O1	1.936(1) Å×2			Mn-O1	1.911(1) Å×2		
Mn-O2	1.948(1) Å×2			Mn-O2	1.960(1) Å×2		
Mn-O2	1.943(1) Å×2			Mn-O2	1.953(1) Å×2		
Mn-O-Mn angles				*Mn-O-Mn angles*			
Mn-O1-Mn	157.5°			Mn-O1-Mn	156.3°		
Mn-O2-Mn	157.0°			Mn-O2-Mn	157.3°		
$\Delta_d(10^4)$	0.064			$\Delta_d(10^4)$	1.242		
Reliability factors				*Reliability factors*			
$R_p=3.77\%$				$R_p=4.14\%$			
$R_{wp}=4.84\%$				$R_{wp}=5.37\%$			
$\chi^2=1.71$				$\chi^2=2.03$			

insulating state is in agreement with Goodenough predictions of the CE-type antiferromagnetic state. The discontinuity around 250 K corresponds to the charge order transition. Magnetic fields have little effect on the resistivity, up to 7 T at least. Above T_{CO}, a model of small polaron describes correctly the temperature dependence: $\rho(T)=\rho_0+AT^{1.5}e^{(E/T)}$ with $\rho_0=1.76\times10^{-3}$ Ω cm, $A=1.40\times10^{-8}$, $E=947$ K. At lower temperature, below T_N, a model of variable range hopping is more suitable: $\rho(T)=Ae^{(E/T)^{0.25}}$ with $A=1.84\times10^{-16}$, $E=3.4\times10^{8}$ K. In the intermediate temperature range, there is a gradual change from the polaronic behavior towards the variable range hopping behavior.

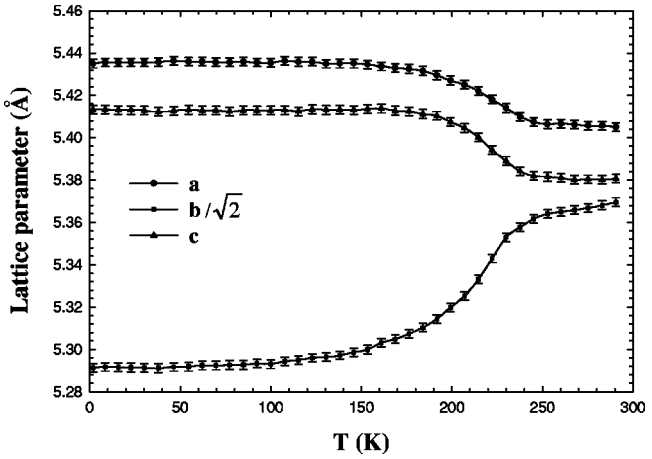

FIG. 3. Lattices parameters of $Nd_{0.5}Ca_{0.5}MnO_3$ as a function of temperature. The charge order transition T_{CO} is indicated by an arrow.

C. Magnetic properties

The dc susceptibility χ_{dc} is plotted in Fig. 7 as a function of temperature. A pronounced peak is visible at 250 K, which corresponds to the charge ordering temperature T_{CO} established by neutron diffraction investigation. Below T_{CO}, the susceptibility is reduced suggesting the occurrence of antiferromagnetic correlations giving no long-range order. On the other hand, no anomaly occurs at the antiferromagnetic

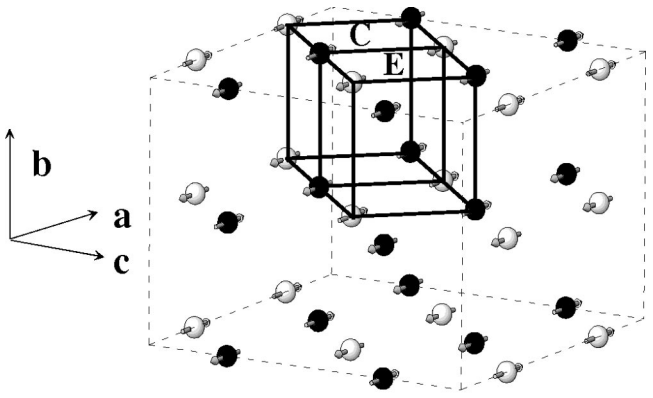

FIG. 4. Representation of the CE-type magnetic structure. This structure is characterized by two Mn sublattices forming ferromagnetic zigzag chains in the *a*-*c* plane.

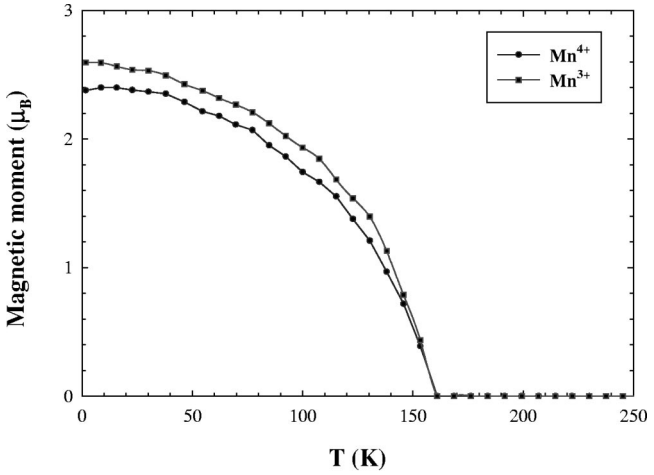

FIG. 5. Magnetic moment of the manganese ions as a function of temperature.

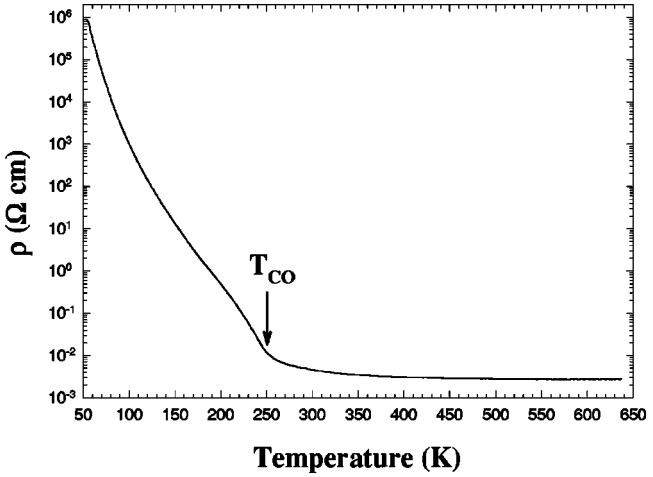

FIG. 6. Electric resistivity as a function of temperature. The antiferromagnetic transition T_N is indicated by an arrow.

ordering temperature T_N determined by neutron diffraction analysis. The increase in χ_{dc} at low temperatures is attributed to Nd^{3+} ions and will be discussed later.

We have also undertaken high-temperature susceptibility measurements up to 800 K using a Faraday balance. The susceptibility follows a Curie-Weiss law with a positive Curie Temperature $\theta_1 = 216$ K indicative of ferromagnetic interactions (Fig. 8). The Curie constant deduced from the linear part of the $\chi_{dc}^{-1}(T)$ curve (450 K$<T<$800 K) gives an effective moment $\mu_{eff} = 5.30\mu_B$. Assuming a rigid coupling of the moments of the Nd^{3+}, Mn^{4+}, and Mn^{3+} ions, one should measure, with 0.5 Nd^{3+}, $0.5Mn^{4+}$, and $0.5Mn^{3+}$ ions per formula unit,

$$\mu_{eff}^{calc} = \sqrt{0.5.\mu_{eff}^2(Nd^{3+}) + 0.5.\mu_{eff}^2(Mn^{3+}) + 0.5.\mu_{eff}^2(Mn^{4+})}.$$

The following assumptions have been made: the electronic levels of Nd^{3+}, at high temperature, are well described by $g = \frac{8}{11}$, $J = \frac{9}{2}$, which leads to $\mu_{eff} = gJ(J+1)\mu_B = 3.62\mu_B$;

TABLE II. Refined magnetic moment components of the Mn^{3+} and Mn^{4+} sublattices. the site coordinates are expressed as fractions of the $(2a \times b \times 2c)$ magnetic cell.

$Nd_{0.5}Ca_{0.5}MnO_3$ 2 K			
$\vec{k}_1 = (0,0,\frac{1}{2})$		$\vec{k}_2 = (\frac{1}{2}0,\frac{1}{2})$	
Mn^{3+}	sublattice	Mn^{4+}	sublattice
Sites	μ_x	Sites	μ_x
$\frac{1}{4}00$	2,6(1)	$00\frac{1}{4}$	−2,4(1)
$\frac{3}{4}00$	2,6(1)	$00\frac{3}{4}$	2,4(1)
$\frac{1}{4}0\frac{1}{2}$	2,6(1)	$\frac{1}{2}0\frac{1}{4}$	2,4(1)
$\frac{3}{4}0\frac{1}{2}$	2,6(1)	$\frac{1}{2}0\frac{3}{4}$	−2,4(1)
$\frac{1}{4}\frac{1}{2}0$	2,6(1)	$0\frac{1}{2}\frac{1}{4}$	2,4(1)
$\frac{3}{4}\frac{1}{2}0$	2,6(1)	$0\frac{1}{2}\frac{3}{4}$	−2,4(1)
$\frac{1}{4}\frac{1}{2}\frac{1}{2}$	2,6(1)	$\frac{1}{2}\frac{1}{2}\frac{1}{4}$	−2,4(1)
$\frac{3}{4}\frac{1}{2}\frac{1}{2}$	2,6(1)	$\frac{1}{2}\frac{1}{2}\frac{3}{4}$	2,4(1)

for Mn^{4+} and Mn^{3+}, the orbital momentum is quenched so that S is the appropriate quantum number: $\mu_{eff} = gS(S+1)\mu_B$, with $g=2$ and $S=\frac{3}{2}$ or 2, which leads to $\mu_{eff} = 3.87\mu_B$ for Mn^{4+} and $\mu_{eff} = 4.90\mu_B$ for Mn^{3+}. This gives $\mu_{eff}^{calc} = 5.10\mu_B$, not far from the experimental value.

dc magnetization measurements were performed up to 22 T. Typical curves are plotted in Fig. 9, one taken above T_{CO}, two others between T_{CO} and T_N, and the last one below T_N. From these data, it seems that the compound presents a magnetic order occurring at the same time as the charge order. A field-induced transition, analogous to a spin flop transition, is clearly visible below T_{CO}. This transition is first order, that is, strongly hysteretic.

We have further analyzed the magnetization curves in terms of Brillouin function, above the ''spin flop field,'' by plotting the magnetization M as a function of H_i/T where H_i is the internal field: $H_i = H_a + H_m$, H_a is the applied field and H_m the molecular field due to the magnetic interactions, proportional to the magnetization. All the curves in the temperature range 290–170 K collapse on a single curve at high field with the following fitting parameters: the Curie temperature is $\theta_2 = 175$ K and the effective moment is $5.83\mu_B$. It should be noted that this analysis is made in the temperature range where χ_{dc} slightly departs from the high-

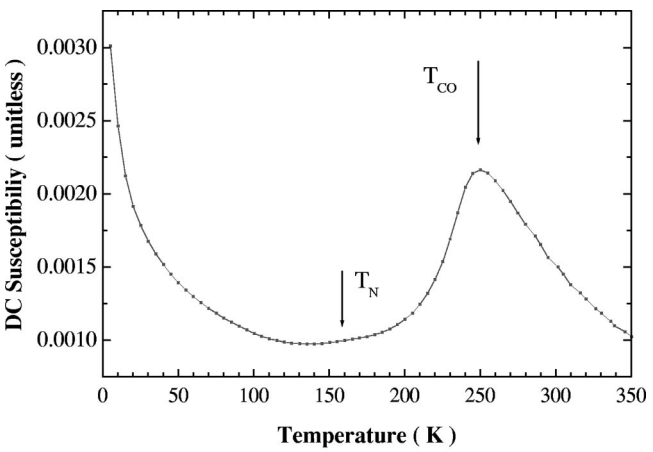

FIG. 7. dc susceptibility (10 mT) as a function of temperature.

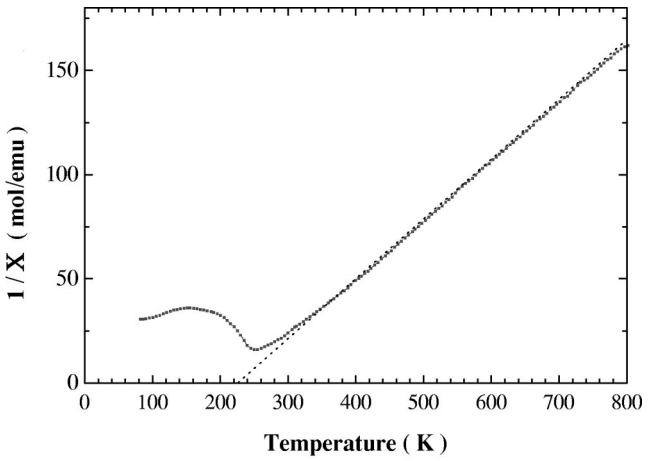

FIG. 8. Inverse of the susceptibility at high temperature. The dotted line is a linear fit giving a Curie temperature $\theta_1 = 216$ K and an effective moment $\mu_{eff} = 5.30\mu_B$.

temperature Curie-Weiss law (Fig. 8). This would indicate that the susceptibility could be described with two Curie-Weiss laws, one with $\theta_2 = 175$ K, $\mu_{eff} = 5.83\mu_B$ for the temperature range 170 K$< T <$290 K and for high magnetic fields, and the other one with $\theta_1 = 210$ K$\simeq T_{CO}$, $\mu_{eff} = 5.30\mu_B$ for $T > 400$ K.

As the temperature is lowered, the influence of the neodymium ions becomes visible in the magnetic response of the compound: the susceptibility increases at low temperature while the magnetization does not saturate. It is however quite difficult to estimate exactly the neodymium contribution at these temperature because of crystal field effects on the Nd electronic level. For instance, in $NdGaO_3$[19] which has a similar perovskite structure, the $J = 9/2$ electronic level is split into five Kramer doublets separated by 137, 133, 363, and 183 K so that only the fundamental level with effective spin 1/2 is occupied at low temperature. This will give a smaller effective moment and a strong deviation from a Curie law. This is exactly what is observed at low temperature in the magnetic susceptibility (see Fig. 7).

IV. DISCUSSION

From the neutron diffraction and magnetization data, we can extract a phase diagram (Fig. 10). The paramagnetic phase (P), above T_{CO}, is a Jahn-Teller distorted phase. It is an insulator with a thermally activated behavior. At low temperature, below T_N, an antiferromagnetic phase (AF-O) with complete charge and orbital ordering is present. Ferromagnetic zigzag chains of Mn^{3+} and Mn^{4+} are formed in the a-c plane. The Jahn-Teller distortion of the Mn-O_6 octahedra has considerably increased. At the same time, the electrical resistivity reflects some kind of disorder: a variable range hopping regime prevails. In the intermediate temperature range Mn^{3+} and Mn^{4+} are ordered, giving rise to a doubling of the a lattice parameter, while the orbital ordering is progressively established. It is clear that two different charge ordered phases are present: a charge ordered phase with no long-range magnetic order in the temperature range $T_N < T < T_{CO}$, and a long-range antiferromagnetic phase with complete orbital ordering for $T < T_N$. Both phases have similar

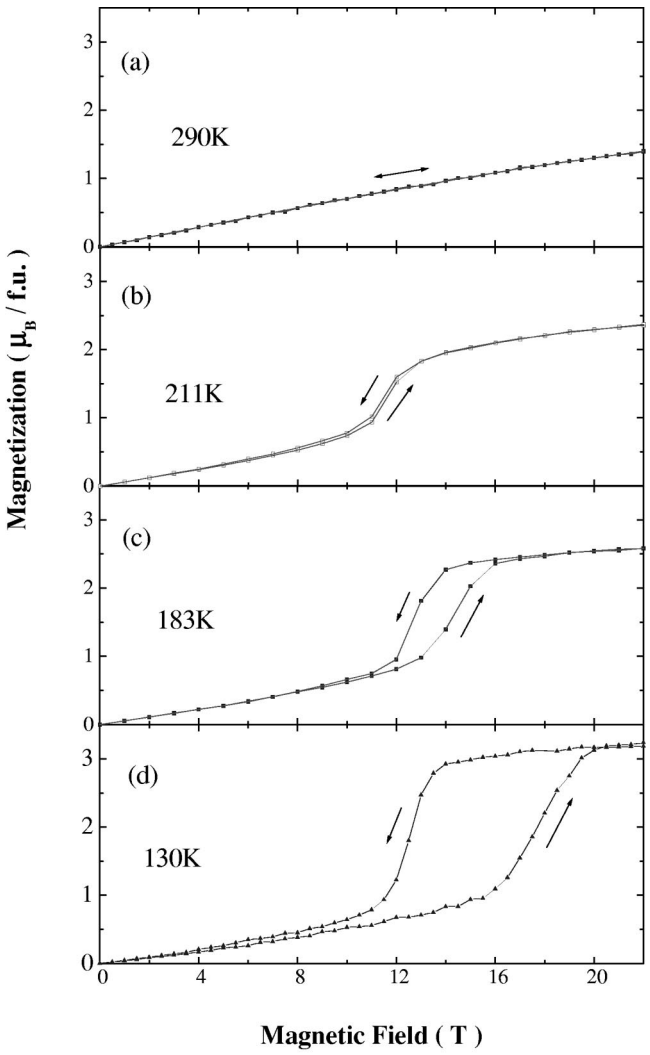

FIG. 9. dc magnetization as a function of magnetic field: (a) $T = 290$ K (paramagnetic domain), (b) $T = 211$ K and (c) $T = 183$ K (charge order domain), (d) $T = 130$ K (antiferromagnetic domain).

response to magnetic field: at low field, they are characterized by a small magnetic susceptibility. At higher field, both phases present a spin flop transition, with a first-order character; the charge ordered state is then destroyed by the magnetic field and a ferromagnetic state prevails.

In Fig. 11, we have plotted the magnetization of this ferromagnetic phase as a function of temperature, for two different fields: 15 T and 20 T deduced from the $M(H)$ curves. The maximum at T_{CO} has been completely removed, which confirms that it is associated with the charge ordering transition. We can distinguish two different contributions to the magnetization: one arises from the neodymium ions, the other one from the manganese ions.

The neodymium ions are paramagnetic (no magnetic order has been detected by neutron diffraction in this temperature range). Their magnetic moment is no longer described by $g = \frac{8}{11}$, $J = \frac{9}{2}$ as has been already mentioned. Using the experimental data on $NdGaO_3$,[19] we can estimate their contribution at 40 K: $M(15\ T) \simeq 0.24\mu_B$, and $M(20$ T$) \simeq 0.32\mu_B$ per formula unit. Experimentally, we get $M(15$ T$) \simeq 3.6\mu_B$ and $M(20$ T$) \simeq 3.8\mu_B$. The gap can

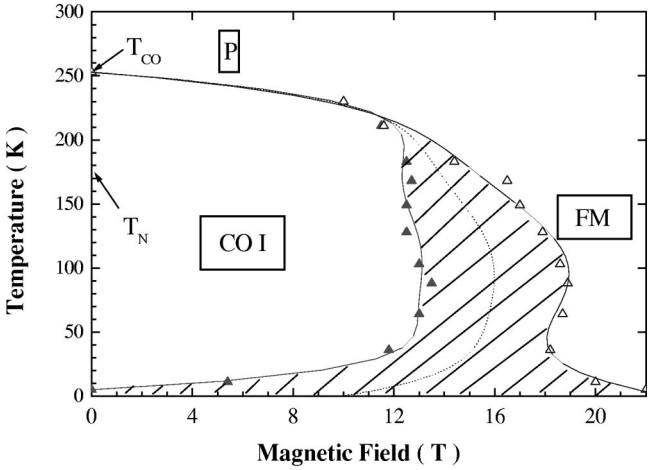

FIG. 10. Magnetic phase diagram of $Nd_{0.5}Ca_{0.5}MnO_3$. T_{CO} and T_N are determined from neutron-diffraction data. The different lines are guides to the eyes to separate the different phases: paramagnetic (P), charge ordered (CO), antiferromagnetic, orbital ordered (AF-O), and ferromagnetic (FM) phases. The dotted line corresponds to the average spin flop field.

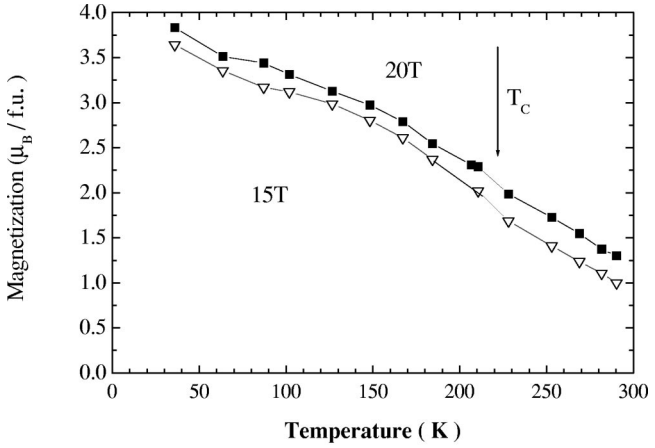

FIG. 11. Magnetization as a function of temperature for the high-field ferromagnetic phase at 20 T and 15 T.

therefore reasonably be attributed to the neodymium ions, which leaves a value of $3.5\mu_B$ for the manganese ions: this is exactly the expected saturated magnetic moment for 0.5 Mn^{4+} and 0.5 Mn^{3+}.

The ferromagnetic phase has then a conventional behavior: in the paramagnetic regime, a Curie-Weiss law is observed with an effective moment $5.30\mu_B$ close to the theoretical one and with a Curie temperature $\theta_1=216$ K. The ordering temperature coincides with the Curie temperature $T_C\simeq\theta_1$. All these results suggests an isotropic ferromagnetic exchange interaction between each Mn^{4+} and Mn^{3+} ion, in agreement with the double exchange model. At low temperature, all the manganese magnetic moments are aligned with a net magnetization of $3.5\mu_B$. Around the magnetic transition, the system is best described by $\theta_2=175$ K and $\mu_{eff}=5.83\mu_B$, revealing the presence of antiferromagnetic correlations.

The low-field, charge ordered phase is much more unconventional: whereas magnetization measurements suggest that $T_N=T_{CO}$, neutron-diffraction measurements clearly demonstrate that the antiferromagnetic order is only established 100 K below T_{CO}. A huge peak in the susceptibility is observed at T_{CO}, as well as a jump in the magnetization as a function of field while no additional lines appear in the neutron-diffraction spectra above T_N.

We can reconcile all the experimental results as follows.

When lowering the temperature from room temperature, the susceptibility first increases due to the formation of a ferromagnetic phase. But this tendency to ferromagnetic order is destroyed by charge ordering that favors antiferromagnetism. The quenching of the double exchange interaction is responsible for the susceptibility peak at T_{CO} as was proposed already in Ref. 9. In the temperature range $T_N<T<T_{CO}$, orbital ordering sets in progressively; it is only achieved around 160 K where long-range magnetic order is established. This is suggested by the temperature variation of the lattice parameters: as the temperature is lowered from T_{CO}, they progressively decrease and remain constant only below T_N. In this picture, when $T_N<T<T_{CO}$, the manganese ions are charge ordered without complete orbital ordering. Several hypotheses remain.

The first one is that T_{CO} corresponds to a magnetic transition towards some unconventional magnetic order, such as modulated or helicoidal phase or noncommensurate phase, $T_{CO}\simeq T_{N1}$, and T_N corresponds to a commensurate magnetic order. There are some experimental evidences, in electron microscopy measurements, that the charge ordered state has a noncommensurable structure in the temperature range $T_N<T<T_{CO}$.

The second hypothesis is that it is not a long-range magnetic order but rather fluctuations that are present: ferromagnetic fluctuations above T_{CO} and increasing antiferromagnetic fluctuations together with decreasing ferromagnetic fluctuations below T_{CO}, giving rise to the susceptibility peak at T_{CO}. A similar behavior has been observed in $Bi_{0.18}Ca_{0.82}MnO_3$:[20] ferromagnetic fluctuations have been observed above the charge order transition T_{CO} but disappear at T_{CO} while antiferromagnetic correlations set in. A long-range antiferromagnetic order was found at lower temperature.

A third hypothesis is that there is a mixture of the ferromagnetic phase and the charge ordered phase. Similar mixing of phases has been observed in $La_{0.5}Ca_{0.5}MnO_3$ using NMR:[21] antiferromagnetic and ferromagnetic domains are found to coexist at all temperatures below the first formation of charge ordered state.

The first hypothesis should be disregarded since no additional peak was observed in the high-resolution neutron-diffraction patterns. Besides, recent electron spin resonance measurements on the same $Nd_{0.5}Ca_{0.5}MnO_3$ compound[22] are in favor of the second hypothesis: the charge ordered phase is characterized by strong magnetic fluctuations with no long-range magnetic order.

V. CONCLUSIONS

Combining neutron diffraction, electric transport, and magnetization measurements, we have obtained a detailed description of $Nd_{0.5}Ca_{0.5}MnO_3$ phase diagram. We have shown that, in the compound $Nd_{0.5}Ca_{0.5}MnO_3$, the paramagnetic regime above $T_{CO}=250$ K corresponds to the progres-

sive establishment of a ferromagnetic phase with $T_C \simeq \theta_1 \simeq T_{CO}$.

From neutron diffraction experiments, a long-range antiferromagnetic phase is observed only below $T_N = 160$ K. Then the manganese ions form ferromagnetic zigzag chains coupled antiferromagnetically (CE type of ordering). The Jahn-Teller distortion is greatly enhanced and complete orbital ordering is established. The compound remains insulating.

A more complicated phase exists between T_N and T_{CO}. In this phase, orbital ordering sets in progressively, antiferromagnetic and ferromagnetic interactions compete. At low magnetic field, a nonmagnetic, insulating state prevails whereas at high magnetic field the ferromagnetic state is favored. The transition towards the ferromagnetic phase, from the nonmagnetic as well as the magnetic charge ordered phase is strongly hysteretic revealing a first-order-type transition.

ACKNOWLEDGMENTS

One of the authors (F.M.) thanks O. Isnard and E. Suard for the neutron diffraction data collected on the D1b diffractometer. We also acknowledge V. Caignaert for helpful discussion on the neutron diffraction results. The Grenoble High Magnetic Field Laboratory is Laboratoire Conventionné à l'Université Joseph Fourier.

*Present address: Inorganic Chemistry Laboratory, South Parks, Oxford OX1 3QR, England.
†Corresponding author.

[1] S.T. Jin, T.H. Tielfel, M. McCormack, R.A. Fastnacht, R. Ramesh, and L.H. Chen, Science **264**, 413 (1994).
[2] Y. Tomioka, A. Asamitsu, Y. Moritomo, H. Kuwahara, and Y. Tokura, Phys. Rev. Lett. **74**, 5108 (1995).
[3] H. Kuwahara, Y. Tomioka, A. Asamitsu, Y. Moritomo, and Y. Tokura, Science **270**, 961 (1995).
[4] N. Kumar and C.N.R. Rao, J. Solid State Chem. **129**, 363 (1997).
[5] V. Caignaert, F. Millange, M. Hervieu, E. Suard, and B. Raveau, Solid State Commun. **99**, 173 (1996).
[6] H.Y. Hwang, S-W. Cheong, P.G. Radaelli, M. Marezio, and B. Batlogg, Phys. Rev. Lett. **75**, 914 (1995).
[7] Y. Tokura, H. Kuwahara, Y. Moritomo, Y. Tomioka, and A. Asamitsu, Phys. Rev. Lett. **76**, 3184 (1996).
[8] C. Zener, Phys. Rev. **82**, 103 (1951); P.W. Anderson and H. Hasegawa, *ibid.* **100**, 675 (1955).
[9] E. Pollert, S. Krupicka, and E. Kuzmicová, J. Phys. Chem. Solids **43**, 1137 (1982).
[10] Z. Jirák, S. Krupika, Z. Šimša, M. Dlouhá, and S. Vratislav, J. Magn. Magn. Mater. **53**, 153 (1985).
[11] Y. Okimoto, Y. Tomioka, Y. Onose, Y. Otsuka, and Y. Tokura, Phys. Rev. B **59**, 7401 (1999).
[12] F. Millange, Ph.D. thesis, Université de Caen, 1998.
[13] J. Rodriquez-Carvajal (unpublished).
[14] O. Richard, W. Schuddinck, G. Van Tendeloo, F. Millange, M. Hervieu, V. Caignaert, and B. Raveau, Acta Crystallogr., Sect. A: Found. Crystallogr. **A55**, 704 (1999).
[15] P.G. Radaelli, D.E. Cox, M. Marezio, and S-W. Cheong, Phys. Rev. B **55**, 3015 (1997).
[16] E.O. Wollan and W.C. Koehler, Phys. Rev. **100**, 545 (1955).
[17] J.B. Goodenough, Phys. Rev. **100**, 564 (1955); **124**, 573 (1961).
[18] S. Satpathy, Phys. Rev. Lett. **76**, 960 (1996); J.L. García-Muñoz, M. Suaaidi, and J. Fontcuberta, Phys. Rev. B **55**, 34 (1997).
[19] A. Podlesnyak, S. Rosenkranz, F. Fauth, W. Marti, A. Furrer, A. Mirmelstein, and H.J. Scheel, J. Phys.: Condens. Matter **5**, 8973 (1993).
[20] Wei Bao, J.D. Axe, C.H. Chen, and S-W. Cheong, Phys. Rev. Lett. **78**, 543 (1997).
[21] G. Allodi, R. DeRenzi, F. Licci, and M.W. Pieper, Phys. Rev. Lett. **81**, 4736 (1998).
[22] F. Dupont, F. Millange, S. de Brion, and G. Chouteau (unpublished).